

Entangled two-photon absorption for the continuous generation of excited state populations in plasma

David R. Smith,^{1, a)} Matthias Beuting,¹ Daniel J. Den Hartog,¹ Benedikt Geiger,¹ Scott T. Sanders,¹ Xuting Yang,¹ and Jennifer T. Choy¹

University of Wisconsin-Madison, Madison, WI

(Dated: 16 September 2024)

Entangled two-photon absorption (ETPA) may be a viable technique to continuously drive an excited state population in plasma for high-bandwidth spectroscopy measurements of localized plasma turbulence or impurity density. Classical two-photon absorption commonly requires a high-intensity, pulsed laser, but entangled photons with short entanglement time and high time correlation may allow for ETPA using a lower intensity, continuous-wave laser. Notably, ETPA with non-collinear entangled photon generation allows for cross-beam spatial localization of the absorption or fluorescence signal using a single laser source. Entangled photon generation, the ETPA cross-section, candidate transitions for an Ar-II species, and plans for a proof-of-principle measurement in a helicon plasma are discussed.

I. INTRODUCTION

Plasma spectroscopy for magnetic fusion energy¹ typically observes collisionally excited intrinsic impurities, injected impurities, or injected neutral beams via absorption or fluorescence collection. These measurements offer spatially resolved information on plasma dynamics and composition limited by the excitation volume and collection optics. Laser-induced fluorescence (LIF), especially in combination with multi-photon processes, allows for more-localized excitation by driving an excited state population with a laser source and observing the associated fluorescence²⁻⁴. For instance, local neutral density measurements in plasma have been demonstrated with two-photon absorption laser-induced fluorescence (TALIF)⁵⁻⁹. For hydrogen TALIF, a $\lambda = 205.2$ nm source drives the $n = 1 \rightarrow 3$ transition (102.6 nm), and the $n = 3 \rightarrow 2$ fluorescence (656.5 nm) is observed.

For multi-photon spectroscopy in plasmas, improved spatial resolution often comes at the expense of poorer measurement signal-to-noise and bandwidth. The two-photon absorption (TPA) rate scales quadratically with photon flux for classical (coherent) light due to uncorrelated photon arrival, but the classical TPA cross-section is very small. Sufficient classical TPA rates require a pulsed laser (repetition rate ~ 10 Hz–100 kHz) with high peak photon flux to leverage the quadratic scaling and overcome the small classical TPA cross-section. However, continuous TPA with a narrow-linewidth CW (continuous-wave) source would be desirable for high bandwidth (\sim MHz) spectroscopy measurements of plasma turbulence and impurity density (Figure 1), and that is the topic of this paper.

Entangled two-photon absorption (ETPA)¹⁰⁻¹³ may be a viable technique to continuously drive¹⁴ an excited state population in plasma. In contrast to classical light, entangled photon pairs are highly correlated which leads

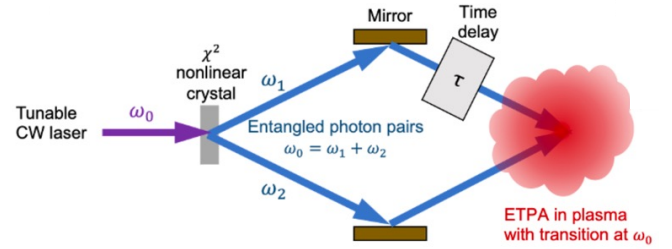


FIG. 1. Illustration of an experimental configuration for ETPA measurements in plasmas.

to the ETPA rate scaling linearly with photon flux. In addition, high time-correlation for entangled photons enhances the ETPA cross-section relative to the classical TPA cross-section. In this paper, we explore the feasibility to continuously drive an excited state population with ETPA and a CW laser to support high-bandwidth spectroscopy measurements of plasma turbulence and impurity density. Additional details of ETPA and entangled photon generation are given in Section II. Section III describes candidate two-photon transitions for an Ar-II (Ar+1) species in a ~ 1 –4 eV laboratory plasma. Finally, Section IV provides a summary and future directions.

II. ETPA ABSORPTION RATES AND ENTANGLED PHOTON GENERATION

Classical TPA involves the excitation from a lower energy state to an excited state by sequential absorption of two (uncorrelated) photons through a virtual intermediate state (Figure 2)¹⁵. The TPA rate per atom (units 1/s) for classical photons is $R = \sigma_c \phi^2$ where $\phi = I/hf$ is the photon flux, $I = \frac{1}{2} c \epsilon_0 E^2$ is the field intensity, σ_c is the classical TPA cross-section (units $L^4 T$). As previously mentioned, small $\sigma_c \approx 10^{-48}$ $\text{cm}^4 \text{s}$ and the quadratic scaling with ϕ typically require a high intensity, short-

^{a)}Electronic mail: david.smith@wisc.edu

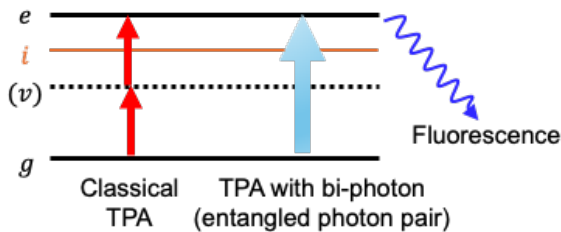


FIG. 2. Energy-level diagram in a TPA process, in which two photons are involved in the excitation from a lower-energy ground state (g) to a higher-energy state (e). A short-lived, virtual state (v) is briefly populated in classical TPA, and this state may have neighboring real intermediate energy states (i) for which single-photon transitions are allowed. In ETPA, the involved photon pair (bi-photon) is strongly correlated.

pulse laser source. For example, an 1-W CW laser with a focal spot diameter of $10\ \mu\text{m}$ corresponds to a photon flux of about 10^{28} photons/ m^2/s , so the classical TPA rate per atom is $\sim 10^8$ 1/s. In contrast, a pulsed laser with an equivalent (1 W) average power, 100 mJ/pulse, 100 ps pulse width, and 10 Hz repetition rate generates the same average photon flux as the CW laser, but the peak power and peak photon flux are 10^9 higher and the average classical TPA rate per atom is $\sim 10^{17}$ 1/s.

ETPA utilizes an entangled photon pair (sometimes called a “bi-photon”) in which the involved photons have strong correlations in their arrival time, momentum, energy, and polarization. Excitation from lower to higher energy states through ETPA can be considered as a single absorption event, leading to a linear scaling in the absorption rate with respect to incident light intensity¹⁵.

The ETPA rate for entangled photons is¹⁶

$$R = \sigma_e \phi + \sigma_c \phi^2 \quad (1)$$

where σ_e is the ETPA cross-section (units L^2). At low entangled photon flux, the ETPA linear scaling with ϕ can dominate the classical TPA quadratic scaling with ϕ^2 . Heuristically, the ETPA cross section is estimated to be

$$\sigma_e \approx \frac{\sigma_c}{A_e \tau_e} \quad (2)$$

where A_e is the entangled area (beam cross section) and τ_e is the entangled photon correlation time (or entanglement time)^{10,17–21}. As described below, τ_e is the inverse of the large bandwidth of entangled photons, so τ_e is very short and σ_e is strongly enhanced. Also, when the entangled photons converge at the target, small A_e further enhances σ_e .

Entangled photon pairs with time-energy (frequency) entanglement can be created by spontaneous parametric down-conversion (SPDC) of a pump laser^{22–25}. Energy conservation ensures that an entangled photon pair retains the pump beam energy, $f_p = f_1 + f_2$ where f_p is the

pump photon frequency, and the pump beam linewidth, $\delta f_p = \delta(f_1 + f_2)$. However, the frequencies f_1 and f_2 of the entangled photons are generally broadband with large $\Delta f = f_2 - f_1$ set by the optics. The short entanglement correlation time τ_e is set by the large bandwidth Δf :

$$\tau_e \equiv \text{FFT}(\Delta f) = \Delta t = t_2 - t_1. \quad (3)$$

The simultaneous properties of short correlation time τ_e and narrow-band total energy $\delta(f_1 + f_2)$ for entangled photon pairs may seem to violate a time-energy uncertainty limit, but the correlation time and total energy are decoupled (commute) for the entangled photon pair and are not subject to a joint uncertainty limit.

As an example, consider a target species with a classical TPA cross-section $\sigma_c = 10^{-48}$ cm^4/s . With an entanglement area $A_e = (10^{-3} \text{ cm})^2$ and a 10 fs entanglement time (corresponding to a ~ 20 nm linewidth), the ETPA cross-section is $\sigma_e \approx 10^{-28}$ cm^2 .

Note that correlation time and photon correlation refer to different statistical properties. The correlation time τ_e is the characteristic width of the second-order coherence $g^{(2)}(\tau)$ where $\tau = t_2 - t_1$ is the delay time. The photon correlation is the second-order coherence at zero time delay, $g^{(2)}(0)$, and it possesses no upper bound. For coherent (classical) light with uncorrelated photons, $g^{(2)}(\tau) = 1$ (the classical lower bound). For highly correlated entangled photons, $g^{(2)}(0) \gg 1$. Short τ_e increases the ETPA cross-section σ_e , but the large correlation $g^{(2)}(0) \gg 1$ leads to the ETPA rate scaling linearly with photon flux. Also, note that large photon correlation $g^{(2)}(0) \gg 1$ is not restricted to entangled photon pairs nor is it inherently a quantum phenomenon. “Squeezed” light with reduced phase fluctuations and enhanced field amplitude fluctuations also exhibits enhanced photon correlation and a TPA rate that scales linearly with photon flux²⁶.

Entangled photons generated by SPDC^{22–25} can be either collinear or non-collinear. Also, the entangled photons have parallel polarization for type-I SPDC and perpendicular polarization for type-II SPDC. Therefore, the ETPA configuration can either be along a single beam path or localized at a cross-beam intersection. Single-photon absorption or classical TPA along a single beam path can be susceptible to spurious reflections of fluorescing light that impair measurement localization and interpretation. Classical TPA with a single laser wavelength can drive TPA along the beam path with the potential for spurious reflections, but a sharp beam waist concentrates TPA at the waist²⁷. However, classical TPA with different wavelength lasers would allow for cross-beam localization such that any observed fluorescence would have originated at the cross-beam intersection. ETPA with non-collinear SPDC, on the other hand, allows for cross-beam localization with a single pump laser source, so again, any observed fluorescence would have originated at the cross-beam intersection. Finally, we note that demonstration of CW ETPA has been reported in chromophore solutions in Ref. 14. Entangled photons were

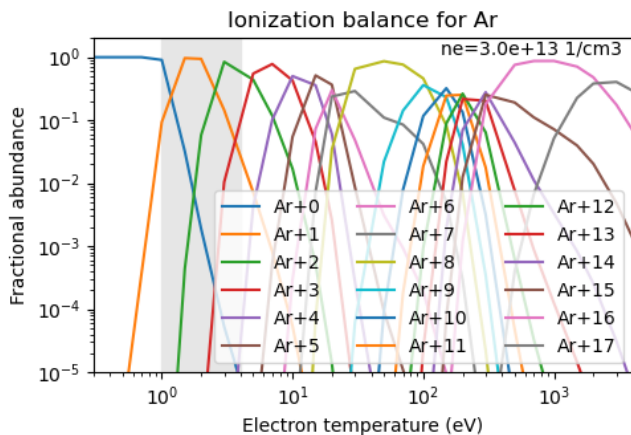


FIG. 3. The fractional abundance of Ar charge states as a function of electron temperature for $n_e = 3 \times 10^{13} \text{ 1/cm}^3$. The grey box marks 1–4 eV which is characteristic of a helicon plasma source.

produced at a rate of 10^7 1/s using a 70 mW CW laser and collinear type-I SPDC.

III. TWO-PHOTON TRANSITIONS FOR AR-II

We consider Argon as a target species for ETPA in plasma because Ar charge states span $\sim \text{eV}$ laboratory plasmas and $\sim \text{keV}$ fusion plasmas, as shown in Figure 3. Also, Ar is a common working gas in laboratory plasmas and a common injected impurity in fusion plasmas. The ionization balance in Figure 3 uses effective ionization and recombination data for ground state ions from the ADAS atomic data suite²⁸. We aim to demonstrate CW ETPA in a laboratory plasma, and the grey box in Figure 3 corresponds to 1–4 eV for a helicon plasma source. Therefore, we will target two-photon transitions in Ar-II or Ar-III species which cover the temperature range for a $\sim 2\text{--}3 \text{ eV}$ helicon plasma.

A desirable two-photon transition would possess a large intrinsic population in the lower level and a small population in the upper level. Figure 4 shows intrinsic Ar-II populations for LS-resolved levels with electron density $3 \times 10^{13} \text{ 1/cm}^3$ and electron temperature 3 eV for an ADAS collisional-radiative calculation. The calculation includes metastable transitions for the four largest populations in addition to the ground state. Another consideration is the wavelength of the two-photon transition. A pump laser wavelength below 400 nm (above 3 eV) would be desirable to reduce the contribution of electron impact excitation. Concurrently, a wavelength above 350 nm would be desirable for compatibility with a frequency-doubled Ti:Sapphire laser (though higher order harmonics could be considered). A Ti:Sapphire laser is widely tunable over 700–1000 nm, so the frequency doubled output can cover 350–500 nm. Therefore, we nominally target two-photon transitions compatible with

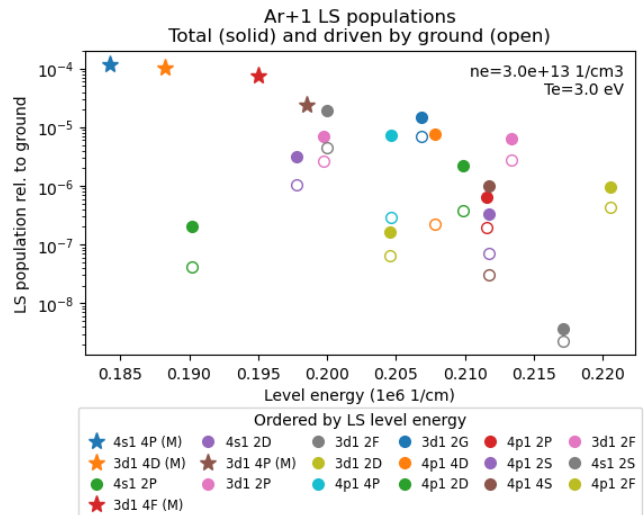


FIG. 4. Collisional-radiative populations for LS-resolve energy levels for the Ar-II ion. Level energies are in f/c wavenumber units. The stars denote metastable populations in addition to ground, the closed circles denote the level population driven by all metastables, and the open circles denote the level population driven by ground. Labels specify the valence electron configuration relative to $[\text{Ne}]3s^23p^4$ and the $2S+1L$ term.

an SPDC pump wavelength range of 350–400 nm.

Finally, the candidate transitions should satisfy selection rules for two-photon transitions. Ar is sufficiently low Z that LS-coupling is the appropriate ordering for spin-orbit interactions (high Z atoms and/or high charge states may require jj-coupling due to strong relativistic effects). Classical two-photon transitions satisfy the selection rules $\Delta S = 0$ and $\Delta L = 0, \pm 2$, with the involved intermediate states obeying selection rules for single-photon transitions. We note that with the use of entangled photon pairs, time-frequency uncertainty can enable intermediate states that are higher energy^{29,30}.

IV. CONCLUSION

In conclusion, we suggest that ETPA may be a feasible technique to continuously drive an excited state population in plasma with a CW laser to support high-bandwidth spectroscopy measurements of plasma turbulence and impurity density. Notably, ETPA with entangled photon generation by non-collinear SPDC allows for cross-beam spatial localization using a single laser source. The ETPA rate scales linearly with photon flux, in contrast to the quadratic scaling for classical TPA, due to high time correlation in entangled photon pair arrival. Also, the ETPA cross-section is enhanced by the short entanglement time. Future work will attempt to demonstrate CW ETPA for an Ar-II or Ar-III two-photon transition in a helicon plasma source. The target transition and entangled photon source will be developed

based on entangled photon generation efficiency, ETPA cross-section and rate, intrinsic energy level populations, and fluorescence intensity.

ACKNOWLEDGMENTS

DRS acknowledges helpful discussions with E. Scime and T. Steinberger. This material is based upon work supported by the U.S. Department of Energy, Office of Science, Office of Fusion Energy Sciences under Award Number DE-SC0024471. Data sharing is not applicable to this article as no new data were created or analyzed in this study.

- ¹E. Pawelec and J. E. T. Contributors, *Eur. Phys. J. Plus* **136**, 838 (2021), number: 8 Publisher: Springer Berlin Heidelberg.
- ²J. Green, O. Schmitz, and M. Zepp, *Physics of Plasmas* **27**, 043511 (2020), publisher: AIP Publishing LLC AIP Publishing.
- ³M. Nikolić, J. Newton, C. I. Sukenik, L. Vušković, and S. Popović, *Journal of Applied Physics* **117**, 023304 (2015), publisher: American Institute of Physics.
- ⁴T. Bieber, S. Bardin, L. d. Poucques, F. Brochard, R. Hugon, J.-L. Vasseur, and J. Bougdira, *Plasma Sources Sci. Technol.* **20**, 015023 (2011).
- ⁵A. Dogariu, S. A. Cohen, P. Jandovitz, S. Vinoth, E. S. Evans, and C. P. S. Swanson, *Review of Scientific Instruments* **93**, 093519 (2022).
- ⁶T. E. Steinberger, J. W. McLaughlin, T. M. Biewer, J. F. Caneses, and E. E. Scime, *Physics of Plasmas* **28**, 082501 (2021).
- ⁷D. Elliott, E. Scime, and Z. Short, *Review of Scientific Instruments* **87**, 11E504 (2016).
- ⁸M. E. Galante, R. M. Magee, and E. E. Scime, *Physics of Plasmas* **21**, 055704 (2014).
- ⁹R. M. Magee, M. E. Galante, D. McCarren, E. E. Scime, R. L. Boivin, N. H. Brooks, R. J. Groebner, D. N. Hill, and G. D. Porter, *Review of Scientific Instruments* **83**, 10D701 (2012), publisher: American Institute of Physics.
- ¹⁰F. Schlawin, *The Journal of Chemical Physics* **160**, 144117 (2024).
- ¹¹A. Eshun, O. Varnavski, J. P. Villabona-Monsalve, R. K. Burdick, and T. I. Goodson, *Acc. Chem. Res.* **55**, 991 (2022), publisher: American Chemical Society.
- ¹²M. G. Raymer, T. Landes, M. Allgaier, S. Merkouche, B. J. Smith, and A. H. Marcus, *Optica* **8**, 757 (2021).
- ¹³R. K. Burdick, G. C. Schatz, and T. Goodson, *J. Am. Chem. Soc.* **143**, 16930 (2021).
- ¹⁴J. P. Villabona-Monsalve, R. K. Burdick, and T. I. Goodson, *J. Phys. Chem. C* **124**, 24526 (2020), publisher: American Chemical Society.
- ¹⁵A. Eshun, O. Varnavski, J. P. Villabona-Monsalve, R. K. Burdick, and T. Goodson III, *Accounts of Chemical Research* **55**, 991 (2022).
- ¹⁶J. Javanainen and P. L. Gould, *Physical Review A* **41**, 5088 (1990).
- ¹⁷M. G. Raymer, T. Landes, and A. H. Marcus, *J. Chem. Phys.* **155**, 081501 (2021).
- ¹⁸K. M. Parzuchowski, A. Mikhaylov, M. D. Mazurek, R. N. Wilson, D. J. Lum, T. Gerrits, C. H. Camp, M. J. Stevens, and R. Jimenez, *Phys. Rev. Appl.* **15**, 044012 (2021), publisher: American Physical Society.
- ¹⁹B. Dayan, A. Pe'er, A. A. Friesem, and Y. Silberberg, *Phys. Rev. Lett.* **94**, 043602 (2005).
- ²⁰A. Joobeur, B. E. A. Saleh, T. S. Larchuk, and M. C. Teich, *Phys. Rev. A* **53**, 4360 (1996).
- ²¹J. Javanainen and P. L. Gould, *Phys. Rev. A* **41**, 5088 (1990).
- ²²C. Zhang, Y.-F. Huang, B.-H. Liu, C.-F. Li, and G.-C. Guo, *Advanced Quantum Technologies* **4**, 2000132 (2021), eprint: <https://onlinelibrary.wiley.com/doi/pdf/10.1002/qute.202000132>.
- ²³N. Schwaller, G. Park, R. Okamoto, and S. Takeuchi, *Phys. Rev. A* **106**, 043719 (2022), publisher: American Physical Society.
- ²⁴C. Couteau, *Contemporary Physics* **59**, 291 (2018), arXiv:1809.00127 [physics, physics:quant-ph].
- ²⁵M. Avenhaus, M. V. Chekhova, L. A. Krivitsky, G. Leuchs, and C. Silberhorn, *Phys. Rev. A* **79**, 043836 (2009), publisher: American Physical Society.
- ²⁶N. P. Georgiades, E. S. Polzik, K. Edamatsu, H. J. Kimble, and A. S. Parkins, *Phys. Rev. Lett.* **75**, 3426 (1995).
- ²⁷N. J. Bednar, J. W. Walewski, and S. T. Sanders, *Appl Spectrosc* **60**, 246 (2006), publisher: SAGE Publications Ltd STM.
- ²⁸<https://www.adas.ac.uk/index.php>.
- ²⁹B. E. Saleh, B. M. Jost, H.-B. Fei, and M. C. Teich, *Physical review letters* **80**, 3483 (1998).
- ³⁰R. K. Burdick, O. Varnavski, A. Molina, L. Upton, P. Zimmerman, and T. Goodson III, *The Journal of Physical Chemistry A* **122**, 8198 (2018).